2008

Imaging of Metal Ion Dissolution and Electrodeposition by Anodic Stripping Voltammetry – Scanning Electrochemical Microscopy

Mario A. Alpuche-Aviles
Mississippi State University

John E. Baur
Illinois State University

David O. Wipf
Mississippi State University, dow1@msstate.edu

Imaging of Metal Ion Dissolution and Electrodeposition by Anodic Stripping Voltammetry – Scanning Electrochemical Microscopy

Mario A. Alpuche-Aviles[†,‡], John E. Baur[§], and David O. Wipf*[,†]

Department of Chemistry, Mississippi State University, Mississippi State, MS 39762
Department of Chemistry, Illinois State University, Normal, IL 61790–4160

*Corresponding author. Fax: (662) 325–1618. E-mail: wipf@ra.msstate.edu

[†]Department of Chemistry, Mississippi State University
[§]Department of Chemistry, Illinois State University
[‡]Present Address: Department of Chemistry,
The Ohio State University, Columbus, OH 43210

Abstract

We have developed a new imaging method for SECM employing fast scan anodic stripping voltammetry (ASV) to provide sensitive and selective imaging of multiple chemical species at interfaces immersed in solution. A rapid CV scan (100 V/s) is used along with a short preconcentration time (300-750 ms) to allow images to be acquired in a normal SECM time frame. A Hg-Pt film electrode is developed having an equivalent Hg thickness of 40 nm that has good sensitivity at short preconcentration times and also retains thin-film behavior with high-speed voltammetric stripping. Fast scan anodic stripping currents are shown to be linear for 1-100 μM of Pb^{2+} and Cd^{2+} solutions using a preconcentration time of 300 ms. SECM images showing the presence of Pb^{2+} and Cd^{2+} at concentrations as low as 1 μM are presented. In addition, a single ASV-SECM image is shown to produce unique concentration maps indicating Cd^{2+} and Pb^{2+}, generated *in situ* from a corroding sample, while simultaneously detecting the depletion of O_2 at this sample. The transient voltammetric response at the film electrode is simulated and shows good agreement with the experimental behavior. We discuss the behavior of images and concentration profiles obtained with different imaging conditions and show that mass-transport limitations in the tip-substrate gap can induce dissolution. ASV-SECM can thus be used to detect and study induced dissolution not only at bulk metal surfaces but also on UPD layers, in this case Cd and Pb on Pt. In addition, we discuss how surface diffusion phenomena may relate to the observed ASV-SECM behavior.

Introduction

Scanning electrochemical microscopy (SECM) has evolved into a very versatile analytical technique for addressing small volumes within the sample diffusion layer.[1, 2] SECM is exceptionally suited for *in situ* studies of interfacial phenomena, e.g., at the solid-liquid interface. In this paper we present a new SECM method to study metal ion concentrations in the sample diffusion layer by combining SECM with fast scan anodic stripping voltammetry (FS-ASV). We demonstrate the capability to image multiple chemical species at high sensitivity. We show that this method has relevance for examining electrodissolution and electrodeposition phenomena at solid/liquid interfaces. We expect that the FS-ASV SECM technique can also be applied to liquid-liquid interface systems or metal toxicity studies of biological samples, both active areas of pursuit in SECM.

In the usual SECM experiment, an image is formed from a three-dimensional set of data points consisting of the scanning tip signal and position coordinates. An image is the graphical representation of the electrochemical data (e.g., current) obtained by the ultramicroelectrode (UME) at every position of the tip scan. This depicts the concentration of only one chemical species. We have recently combined fast-scan cyclic voltammetry (FSCV) and SECM, demonstrating the concept of imaging different chemical species based on their different current-potential-time behavior.[3-5] In FSCV-SECM, the probe collects a voltammogram at every point of the image grid. The potential-time dependence of the current makes it possible to simultaneously detect different electroactive substances. The current-potential-time data obtained as a function of position generates maps of each of the electroactive chemical species. This method can

also be used to detect species that reversibly adsorb and preconcentrate on the surface of the electrode and are then stripped off during a voltammetric scan. Cathodic stripping voltammetry imaging of locally generated Cl^- in solution was demonstrated as a model of adsorption-based detection.[5]

This paper demonstrates that these new imaging possibilities can be further expanded with ASV-SECM. Stripping voltammetry methods are well established analytical techniques used for their selectivity and high sensitivity. In ASV, a preconcentration step reduces metal ions at a Hg electrode to form an amalgam. A stripping voltage sweep in the positive direction causes oxidation of the amalgamated metal. In ASV using Hg thin film or rotating electrodes of traditional size,[6-12] "fast scan" is used to refer to rates of 1 – 10 V/s. However, microelectrodes permit the use of faster voltammetric scan rates—with an attendant analytical advantage.[13, 14] Baranski has reported the use of Hg droplet-coated C-fiber UMEs for ASV of Pb^{2+} and Cd^{2+} at scan rates of 1-100 V/s.[15] In Baranski's work, the log of the peak current was found to vary linearly with the log of the scan rate for a preconcentration time of 60 s, although with different slopes for Cd and Pb (5 and 50 nM/decade for Cd^{2+} and Pb^{2+}, respectively). Numerical simulations of the reversible process at microdisk mercury film electrodes have produced equations giving the peak current, potential, and width for slow scan rates.[16]

Slow-scan ASV has been previously incorporated into SECM. Daniele et al. have used a non-imaging ASV-SECM measurement using Hg UMEs with a 50 mV/s stripping scan to detect solution-phase concentrations of Pb^{2+} and Cu^{2+} near lake sediment.[17, 18] Janotta et al. obtained profiles of Zn^{2+} from a corroding ZnSe sample protected with

diamond-like C and exposed to H_2O_2 using a preconcentration time of 10 s and a potential scan rate 5 mV/s.[19] Rudolph et al. monitored the dissolution of rhodochrosite ($MnCO_3$) in acidic solutions and measured changes in the concentration of Mn^{2+} as a function of time and distance and were able to image the concentration profile over a region of 700×140 μm using a potential scan rate of 50 mV/s.[20] Ruhlig and Schuhmann used stripping of Cu deposited under UPD conditions on the SECM tip to image Cu dissolution at a scan rate of 25 mV/s and preconcentration time of 15 s. Under these conditions, SECM imaging is limited to processes that take place in the time scale of hours.[21]

We wish to avoid the long imaging times resulting from the use of slow stripping scans and long preconcentration times. We show here that imaging times in ASV-SECM can be greatly decreased by employing a FSCV-methodology to make metal-selective images using voltammetry scan rates of 100 V/s and preconcentration times of 300-750 ms. Fast scan rates allow imaging without significantly increasing the acquisition time compared to normal amperometric SECM and can also increase sensitivity. While the imaging time is a function of several parameters (e.g., scan range, step size and raster scan rate), the largest image in this paper(150×200 μm, Figure 6) required a scan time of ~ 20 min. FS-ASV SECM images showed changes in metal ion concentration at surfaces at the micromolar level. The acquisition of a full voltammogram at every point of the image allows simultaneous detection of different species (Pb^{2+}, Cd^{2+}, and O_2). In addition, the preconcentration at the tip allowed unexpected insight into induced metal dissolution at bulk and UPD metal surfaces as well as information about surface diffusion

effects. We also discuss how imaging conditions (e.g. tip-sample separation) affect the experimental images.

Experimental Section

Solution preparation Metal ion solutions for ASV experiments were made daily by dilution from 10 mM stock solutions of $Cd(NO_3)_2$ and $Pb(NO_3)_2$. Both stock and diluted solutions of metal ions were kept in plastic containers. The Cd^{2+} and Pb^{2+} solutions were prepared in filtered 0.5 M KNO_3 (pH ~ 6.2, not adjusted) solutions. All solutions were prepared with 18 MΩ cm water (Nanopure, Barnstead Thermolyne). Before use in the preparation or storing of solutions, glassware was washed with detergent and water and then was soaked in HNO_3 solutions (10 % v/v overnight or 6 M for 1 h) . Plastic containers and the SECM cell were rinsed with 6 M HNO_3.

Electrodes Imaging tips were prepared by electrodeposition of Hg onto 10 μm diam Pt disk electrodes. The Pt electrodes were built from 10 μm diam Pt wire (Goodfellow Metals, Ltd., Cambridge, U.K.) sealed in soft-glass capillaries as reported previously.[22] The electrodes were polished with 0.3 μm alumina before Hg electrodeposition and after Hg removal. The Hg electrodeposition solution was 5.7 mM $HgNO_3$, 1.0 M KNO_3, and 0.5 % v/v conc. HNO_3. Hg films on Pt surfaces were formed by CV at high potential scan rates using two methods: method 1, 300 continuous CVs at 50 V/s were run between the potentials of 0 and –1600 mV vs. MSE; method 2, 90 CVs at 50 V/s were run between 0 and –790 mV vs. MSE. Unless otherwise stated, method 1 was used to prepare Hg-film electrodes.

Electrode substrates were prepared from 10 or 100 μm diam Pt wires (Goodfellow Metals, Ltd.) that were sealed into glass as above and then embedded in Epon 828 epoxy

(Miller-Stephenson, Danbury, CT) using 13 wt % triethylenetetramine hardener (Miller-Stephenson). Dual substrate electrodes were made by connecting two 1 cm lengths of 10 μm diam Pt wire to 30-gauge wire-wrap wire with silver epoxy (H20E, Epotek, Massachusetts); the Pt wires were then affixed to both sides of a 6 μm thick polyethylene-terphthalate film (Goodfellow) and sandwiched with microscope slides; this assembly was cast into epoxy (Epon 828), and sanded to expose two independent disk electrodes with a separation of ca. 25 μm. All substrate electrodes were polished with 0.05 μm alumina before they were used.

The dual Pb and Cd substrates were formed by electrodepositing Pb on one of the Pt substrate electrodes at a potential of –500 mV vs. Ag/AgCl for 500 s in a deaerated, aqueous 1.0 mM $Pb(NO_3)_2$ solution. The electrode was then immediately rinsed with deionized water. Cd was then electroplated on the other electrode at a potential of –1200 mV vs a Pt quasi-reference electrode for 370 s from a solution of 9.5 mM $Cd(NO_3)_2$ and 20.3 mM NH_4I in 2-propanol. The electrode was removed from the solution and rinsed with 2-propanol and acetone. This produced two electrodes of each of the metals (~5 - 10 μm thickness) separated by a ca. 25 μm gap. Upon introduction of the electrode to the aqueous experimental solution, a potential of –1300 mV vs. MSE was immediately applied to prevent metal dissolution.

Reference electrodes were either Ag/AgCl in 3 M KCl or $Hg/HgSO_4$ in saturated K_2SO_4 (MSE). When Ag/AgCl was used for Hg deposition and Hg/Pt-stripping, a packed paper bridge saturated with 1 M HNO_3 was used. Some ASV experiments at lower metal ion concentration (< 100 μM) used a MSE reference electrode.

Instrumentation The SECM instrument used for FS-ASV SECM imaging has been previously described.[5] The potentiostat's low-pass filter was set at 4 kHz during fast scan stripping experiments in quiescent solutions and during imaging to avoid distortion of the voltammograms. During tip positioning, the output of the potentiostat was also routed through a 4 Hz low pass filter to allow better DC current monitoring. A power-line synchronizer was necessary to obtain artifact free images by synchronizing acquisition of the CV current with the ac supply current.[5] Calibration of the tip raster rate (in μm/s) was required to ensure reproducibility of the ASV since the duration of the major axis step sets the preconcentration time (300 – 750 ms). This was accomplished by measuring the time the Burleigh controller took to move a known distance. In some experiments (i.e. in initial line-imaging experiments and SV in quiescent solution), data were acquired with a digital oscilloscope (TDS 540A, Tektronics, Beaverton, Oregon).

Simulations Finite differences simulations of the anodic stripping voltammograms were initially set up in Comsol Multiphysics (version 3.3, Comsol, Burlington, MA) using the diffusion application mode (transient analysis) in two dimensions (axial symmetry). A rectangular simulation space having a width (r_{max}) 100 times the electrode radius and a height (z_{max}) 50 times the electrode radius was used for all simulations. Weak constraints were used to improve the accuracy of the flux calculations and thus reduce the number of grid elements. For simulations of multiple ASV cycles, the models were converted to scripts and run with Comsol Script (version 1.1). Details of the model, initial and boundary conditions, and the simulation parameters can be found in the supplemental information.

Results and Discussion

Mercury Film Tip Electrodes Initial testing of ASV-SECM used hemispherical Hg electrodes; however the protruding Hg surface was prone to damage by contacting surface during an approach of the tip to the substrate. Often, after an accidental crash at a Pt substrate, we observed very sharp stripping peaks in a Pb^{2+} solution as a consequence of the loss of the majority of the Hg and the formation of a Hg film tip electrode. Figure 1 shows the ASV obtained with a 10 μm diam Hg-covered Pt disk after the tip crashed into a 100 μm diam Pt substrate. In this solution of 0.1 mM $Pb(NO_3)_2$ /0.1 M HCl, the stripping peak shows a sharp decay to the baseline indicating thin-film behavior. This accidental result suggested that better control of the Hg deposition process would improve the electrodes used in ASV-SECM.

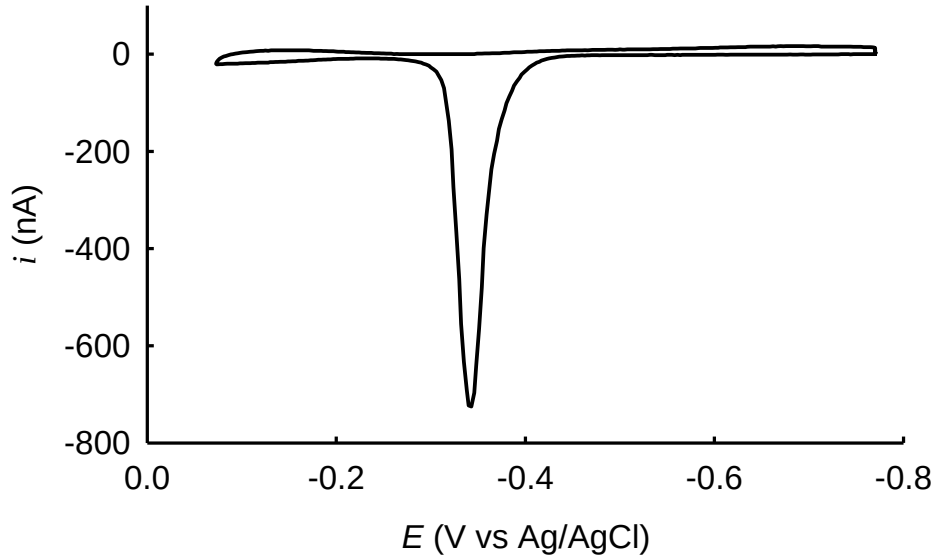

Figure 1. ASV of a 0.1 mM $Pb(NO_3)_2$/0.1 M HCl solution at a hemispherical Hg-coated 10 μm diam Pt disk electrode subsequent to a crash at a 100 μm diam Pt disk substrate.

Our optimized method for electrode preparation, Method 1, consisted of CVs run from a potential just negative of the Hg wave into the H_2 wave. As discussed in the supporting information, this method was developed to circumvent the nucleation and growth of Hg on Pt.[23] The deposited Hg forms an amalgam with Pt[24, 25] but the solubility of Pt in Hg is low (5×10^{-4} at %).[26] From charge measurements and assuming films of pure Hg, the film thickness is 44 ± 9 nm.

Fast Scan Anodic Stripping Voltammograms The behavior of the Hg electrodes under imaging conditions was verified by calibration in quiescent solution. ASV data was acquired by repeating a sweep followed by a 300 ms preconcentration time to replicate imaging conditions. The peak currents were used to generate calibration curves for both Pb^{2+} and Cd^{2+} after background correction. Acquisition of the calibration CVs were also synchronized to the power line phase to further mimic SECM acquisition conditions. Calibration data in 1, 5, 10, 50, 100, 500, and 1000 μM solutions of $Cd(NO_3)_2$ and $Pb(NO_3)_2$ gave linear behavior for concentrations up to 100 μM. Above 100 μM, the curves deviated from linearity and the stripping peaks were often irreproducible (not shown). It was found that some loss of Hg occurred when the electrode was exposed to these higher concentrations and also when the deposition time was longer than a few seconds. In the range of 1 – 100 μM, four example electrodes gave different calibration slopes and intercepts: between 1.5 – 2.0 nA/μM for Pb^{2+} and 1.0 – 1.5 nA/μM for Cd^{2+}. Calibration was therefore necessary for all electrodes used for SECM imaging. Figure 2 shows a Pb^{2+} and Cd^{2+} calibration curve obtained with one of the these electrodes (see Figure S-1A for CV).

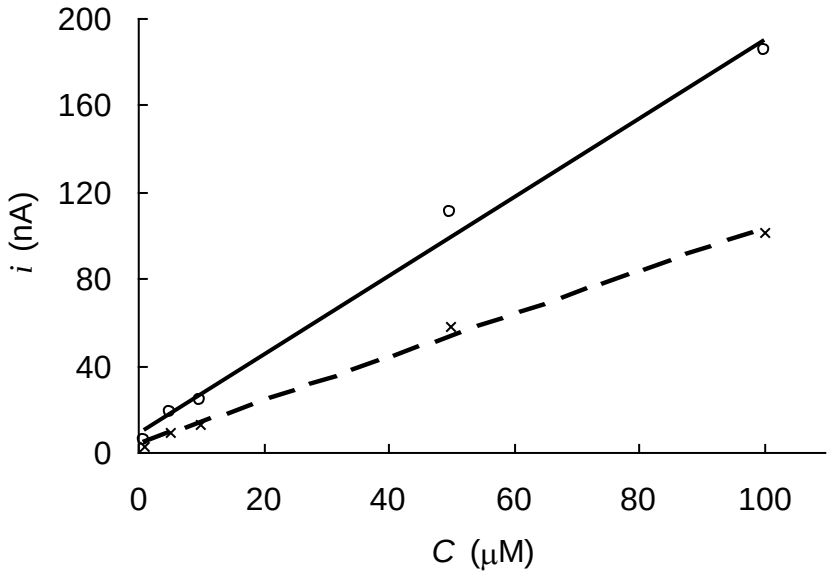

Figure 2. Typical fast-scan ASV calibration curves for Hg-Pt film electrodes. The solutions used were 1, 5, 10, 50, and 100 μM in both Cd^{2+} and Pb^{2+}. Experimental data: (o) for Pb^{2+} and (×) Cd^{2+}, calibration curves: for Pb^{2+} i = 1.82C + 8.31 (—), R^2 = 0.992. For Cd^{2+} i = 0.995C + 3.89 (- - -), R^2 = 0.996. ASV conditions: preconcentration potential of –1.3 V vs MSE, t_p = 300 ms, v = 100 V/s.

We found that the shape of Cd and Pb ASV peaks varied even for evidently identically prepared electrodes. The different appearances of the peaks are probably due to differences in the amount of Hg deposited and subsequently the Hg-Pt amalgam composition and morphology (see Figure S-1 for examples). Also, the use of power-line synchronized data collection may affect peak shape (see Figure S-2)

In our ASV experiments, the Pb stripping peak was always larger than the Cd peak at equal Cd^{2+} and Pb^{2+} concentration. The background subtracted data in Figure 3 illustrates this: after deconvolving the peaks by fitting them to a 3-parameter Gaussian function, the Pb/Cd peak ratio is about 1.7 in a solution of 100 μM Cd^{2+} and Pb^{2+} in 0.5 M KNO_3 at 100 V/s. The peak functions were numerically integrated by the trapezoid

method to find the stripping charge for both metals. The data and analysis from Figure 3 is summarized in Table 1.

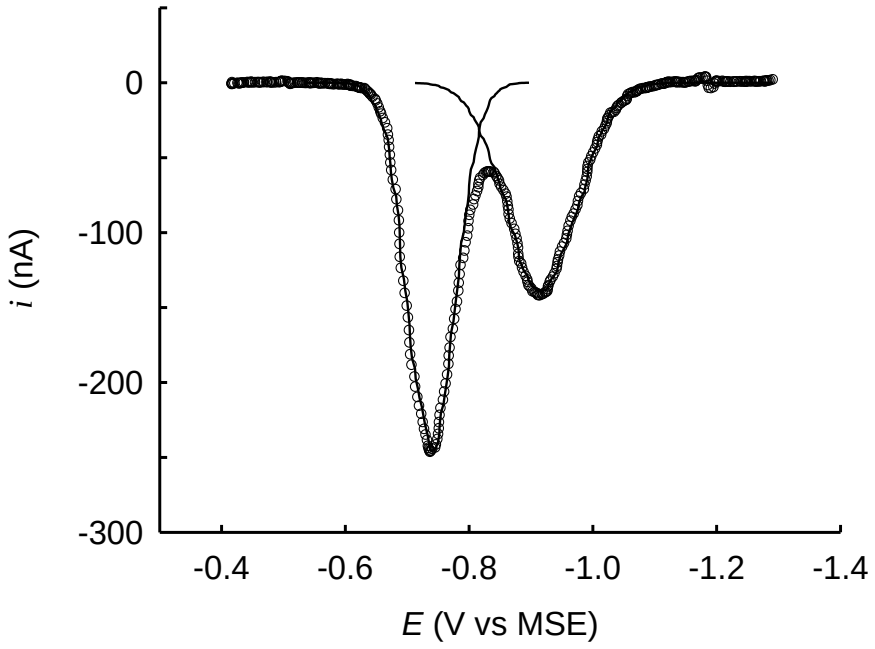

Figure 3. Background subtracted, fast-scan ASV of 100 μM Pb^{2+} and Cd^{2+} in 0.5 M KNO_3 at 100 V/s. (o) experimental data, (—) Gaussian peak fit.

Table 1. Experimental results for the ASV stripping peaks in Figure 3

	i_p (nA)	E_p (mV vs MSE)	E_p-E^0 (mV)	$W_{1/2}$ (mV)	Stripping Charge (pC)	Preconcentration Charge (pC)*	Simulated Charge (pC)
Pb	–246	–735	36	92	240	100.2	219
Cd	–139	–907	96	137	202	117.0	174

*Theoretical for a UME 300 ms transient in 100 μM M Pb^{2+} and Cd^{2+}

There is an obvious difference in the width and amplitude of the experimental peak currents for Pb and Cd. The larger peak half-width potential $W_{1/2}$, and lower stripping peak current (i_p) can be explained by slower dissolution kinetics of Cd

compared to Pb. The charge ratio of Pb/Cd of ~1.19 is due to different Pb^{2+} and Cd^{2+} diffusion coefficients (see Table 2 and supporting information).

Table 2. Standard potential and diffusion coefficient data for Pb and Cd

		$D/10^{-6}$ (cm²/s)		
Reaction	**E^0 (mV vs. NHE)**[36]	**As M^{2+} 0.5 M KNO_3***	**As M^0 in Hg**[37]	**As M^{2+} on Pt surface**[38]
$Pb(Hg) \rightleftharpoons Pb^{2+} + 2e$	–120.5	8.16	14.1	0.00025
$Cd(Hg) \rightleftharpoons Cd^{2+} + 2e$	–352.1	6.86	16.6	0.27

*Diffusion coefficients were interpolated from reported values[26]

The ratio between the amounts of charge (i.e. reduced material) found in the stripping peak and the expected charge from the steady-state preconcentration, ~2.0 is due to a quasi-steady condition state reached during the stripping-preconcentration cycle. During the 300 ms preconcentration step, the electrode reduces metal ions from solution at the mass-transport limit. The metal ions are released to solution by stripping over a period of 6-10 ms. Because the tip potential is swept back to the preconcentration potential; the ions are immediately re-reduced during the subsequent 300 ms preconcentration period. In addition, new ions from the bulk are reduced during the preconcentration step.

Figure 4 shows simulations of the preconcentration-stripping cycles on a Hg film UME (thickness = 44 nm). For different preconcentration times, t_p, both the cathodic and anodic (stripping) currents increase until they reach a constant value after about 10 cycles (Figures 4A and B). For the values of t_p in Figure 4, these 10 cycles correspond to < 4 s of experimental time. Normalizing the final ASV peak by the first ASV peak gives a ratio

between 1.6 and 1.9, depending on t_p (Figure 4C). It is worth noting that this ratio does not increase monotonically with t_p, probably due to the complex relationship between linear and convergent diffusion at shorter and longer times.

Our simulations assume Nerstian behavior and do not predict the shape of the kinetically limited experimental peaks. However, the simulated charge of the stripping metal ions for t_p = 300 ms is within 15% of the experimental results in Figure 3 (summarized in Table 1). The final stripping peak values from the simulations at the 60th cycle is for Pb, i_p = 509 nA Q_p = 219 pC (difference of 9 %), and for a similar simulation for Cd (not shown): i_p = 406 nA Q_p = 174 pC (difference of 14%).

These quiescent ASV simulations and experimental results have implications for imaging and approach-curve ASV-SECM experiments. In both cases, the tip must be allowed to equilibrate with the solution prior to experiment, since the simulations show an initial increase in stripping current and charge with each ASV cycle. The equilibrium i_p is a complex function of t_p and film thickness, thus, quantitative imaging will require calibration for different experimental conditions. Despite the dependence of i_p current on t_p and re-dissolution kinetics, a linear dependence with of i_p with concentration is achieved and used to image changes in concentration within the linear range (1 to 100 μM in this work). Finally, the preconcentration time of the fast ASVs not only improves the limit of detection, but after the tip has reached a quasi steady state, the "sphere of influence" of the tip extends beyond the diffusion layer of a steady state UME. As it will be discussed below, this can induce new tip-substrate interactions to image dissolution phenomena.

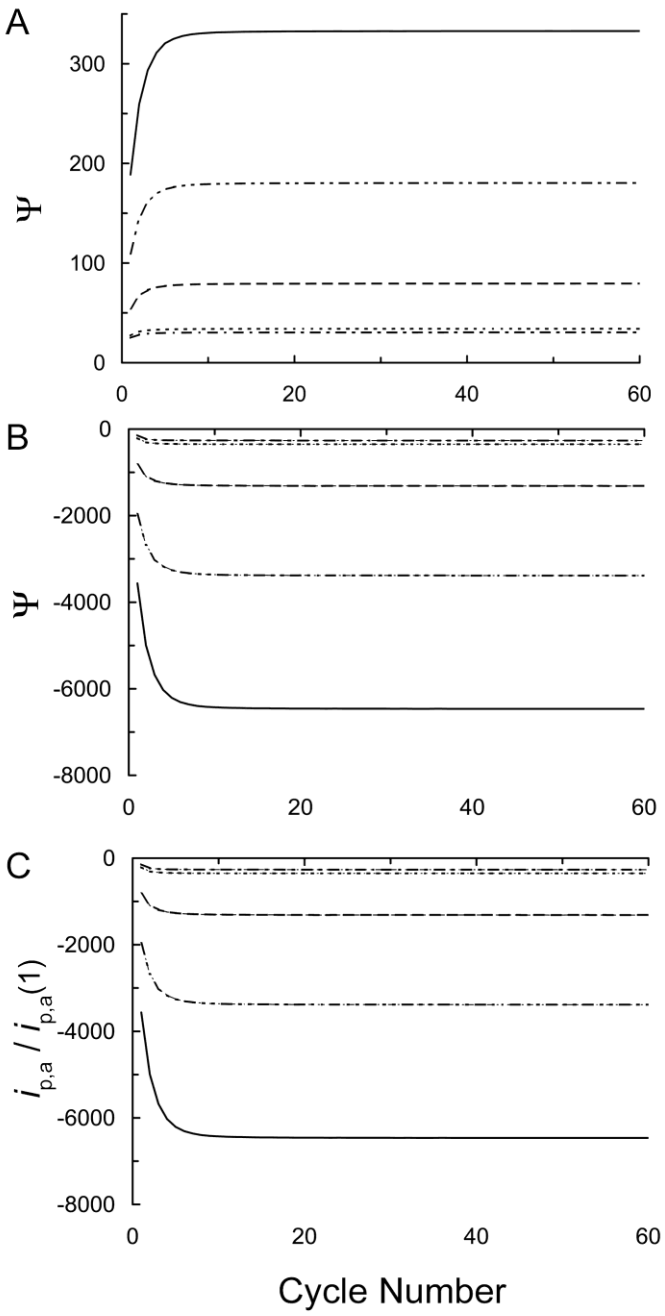

Figure 4. Simulation results for ASVs with different preconcentration times (t_p). (A) reduction currents and (B) stripping anodic (negative) peaks as a function of the numbers of CVs run and (C) the relative increase of the anodic peak $i_{p,a}$ with respect to the first peak value, $i_{p,a}(1)$. Note the different scales. t_p = (–·–) 0 ms, (- - -) 4 ms, (— — —) 50 ms, (–··–··) 150 ms and (——) 300 ms. In (A) and (B) the dimensionless current $\Psi = i/(4nFaDC^*)$.

Imaging with ASV-SECM In ASV-SECM imaging, the tip movement is synchronized to the ASV acquisition. During the time interval in which the tip moves from image point to image point, the tip electrode is set at the preconcentration potential. When the tip arrives at the next image point, a cyclic voltammogram is acquired by sweeping from the preconcentration potential through the stripping peak potentials and then returning to the preconcentration potential. Current-potential data is acquired only during the CV sweep and this data is used to form the ASV-SECM images. In addition, a simultaneous amperometric SECM image is acquired at the preconcentration potential by sampling the tip current just prior to the CV acquisition. For the experiments reported here, the preconcentration time (i.e. the time between successive image points) is 300 to 750 ms and the CV scan rate is 100 V/s. The ratio of the time between CV acquisitions compared to the CV acquisition time (about 16 ms) is between 20-50, usually considered sufficient to permit the diffusional profile to relax back to near steady-state.[27, 28] Thus, both ASV-SECM images and essentially normal amperometric SECM images are acquired during a single image scan. Figure S-3 illustrates the timing relationship between tip position scanning, metal preconcentration, and ASV current-potential acquisition.

Initial ASV-SECM experiments used relatively high test concentrations of the metal ions (0.1 mM Pb^{2+}, Cd^{2+}). Current-distance data were acquired with Hg-film electrodes (method 2) approaching a 100 μm diam Pt substrate. In the data shown in Figure 5, the substrate potential of –0.6 V vs. Ag/AgCl reduces Pb^{2+} at a diffusion-controlled rate. The tip was moved towards the surface of the Pt substrate electrode at 5 μm/s and an ASV was acquired every 300 ms (preconcentration time, t_p). The ASV-

SECM current-distance data are shown with distance (z) as the abscissa, the tip potential (only the anodic sweep) the ordinate, and the stripping current coded in a color map. Three-dimensional data sets of this sort might be more appropriately called approach-surfaces.[3] Approaching the substrate, stripping peaks for both Pb (E_{tip} = –0.36 V) and Cd (E_{tip} = –0.50 V) are present. Near the surface (z <20 μm), the Pb^{2+} peak is greatly diminished due to depletion by the substrate. The Cd^{2+} peak is only slightly affected, since the substrate is reducing it at a slower rate than Pb^{2+}.

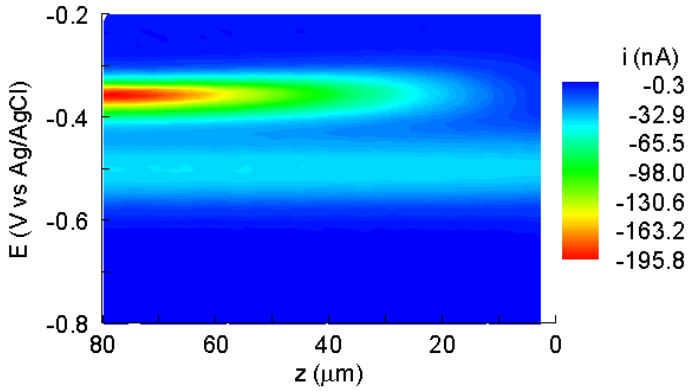

Figure 5. ASV-SECM approach surface for a 10 μm diam Hg-Pt film tip at a 100 μm diam Pt substrate. 100 V/s ASV sweep from -0.8 V (preconcentration voltage) to 0 V vs. Ag/AgCl. Raster scan rate = 5 μm/s, ASVs taken every 1.5 μm, t_p = 300 ms. The substrate is approximately at z = 0.

A complete surface scan consists of a set of current-positions surfaces, one per raster line. The resulting four-dimensional data set cannot be represented on a single graph. These data sets are thus presented as a three-dimensional subset of the data. Here, the current data from a specific potential (and potential scan direction) is plotted versus the tip position (x,y) as a false color plot.[5] Images representing a particular metal ion concentration are generated by plotting the current at the stripping peak potential. The

standard SECM images acquired in parallel by sampling the current at the end of the preconcentration step are plotted as normal (i, x, y) images.

Several precautions must be observed during ASV-SECM imaging. As described above, proper timing of the ASV data with tip movement is crucial in ASV-SECM. We also found very poor baseline and peak current reproducibility if the same sequence of preconcentration potential and stripping voltammetry was not continuously maintained at all times during imaging and also for some time prior to imaging (< 1 min). For example, only the forward position scan across the major axis (e.g. x) was used for the collection of the ASV data but ASV scanning was necessary during the reversed scan and also during the tip increment in the minor axis (e.g. y) direction occurring after the reverse position scan. Also, to improve reproducibility at the lowest concentrations examined, two to three ASVs were run (but not recorded) just prior to the forward positioning scan.

Another precaution is that the potential of the tip electrode must be carefully controlled during preliminary tip positioning. Setting the potential to reduce metal ions even for a few minutes can seriously affect the characteristics of the Hg film. This is probably due to the formation of intermetallic compounds that “overload” the Hg film during extended reduction to the amalgam. The resulting Hg-amalgam film was often completely removed during a subsequent ASV stripping sweep. To avoid this, the Hg-Pt electrode was held at a value positive of the reduction potential of Cd and Pb at Hg during any required non-imaging tip positioning. Just before the collection of the image, the software constantly triggered voltammograms with the same potential range and pre-concentration time (typically 300 ms) set for the image acquisition. The tip current was

monitored with an oscilloscope until the voltammograms became constant before starting imaging experiments.

The imaging capability of ASV-SECM is demonstrated at a dual Pt electrode substrate electroplated with Pb and Cd. The substrate electrode was used to locally generate Cd^{2+} and Pb^{2+} in a 0.5 M KNO_3 solution initially free of metal ions. The images shown on Figure 6 correspond to three electroactive species present in solution: Pb^{2+} (6A, E_t = –703 mV vs. MSE), Cd^{2+} (6B, E_t = –847 mV), and O_2 (6C, E_t = –1298 mV). All three images were generated by plotting the ASV currents at the indicated potentials (all vs. MSE) from a single ASV-SECM imaging scan. Note that the highest anodic currents appear at different regions of the substrate: the maximum image currents for Pb^{2+} are near *x*, *y* coordinates of (115, 120) μm and near (90, 75) μm for Cd^{2+}. Unlike the Pb^{2+} and Cd^{2+} images, the O_2 image shows that O_2 concentration is depleted at the location of both substrate electrodes (Figure 6C). Figure 6D shows that stripping voltammograms at different regions of the *x*-*y* scan differ markedly: small amounts of Pb^{2+} and Cd^{2+} are detected at the initial part of the image, and appear at different relative amounts depending of the position of the scanning tip: showing a maxima in the same positions as in Figure 6A and 6B, consistent with an optical micrograph of the substrate (Figure 6E). A separate calibration experiment gave an estimate of a micromolar concentration of Pb^{2+} and Cd^{2+} in images Figure 6B and 6C, confirming that simultaneous detection of low-concentration metal ions is possible with ASV-SECM.

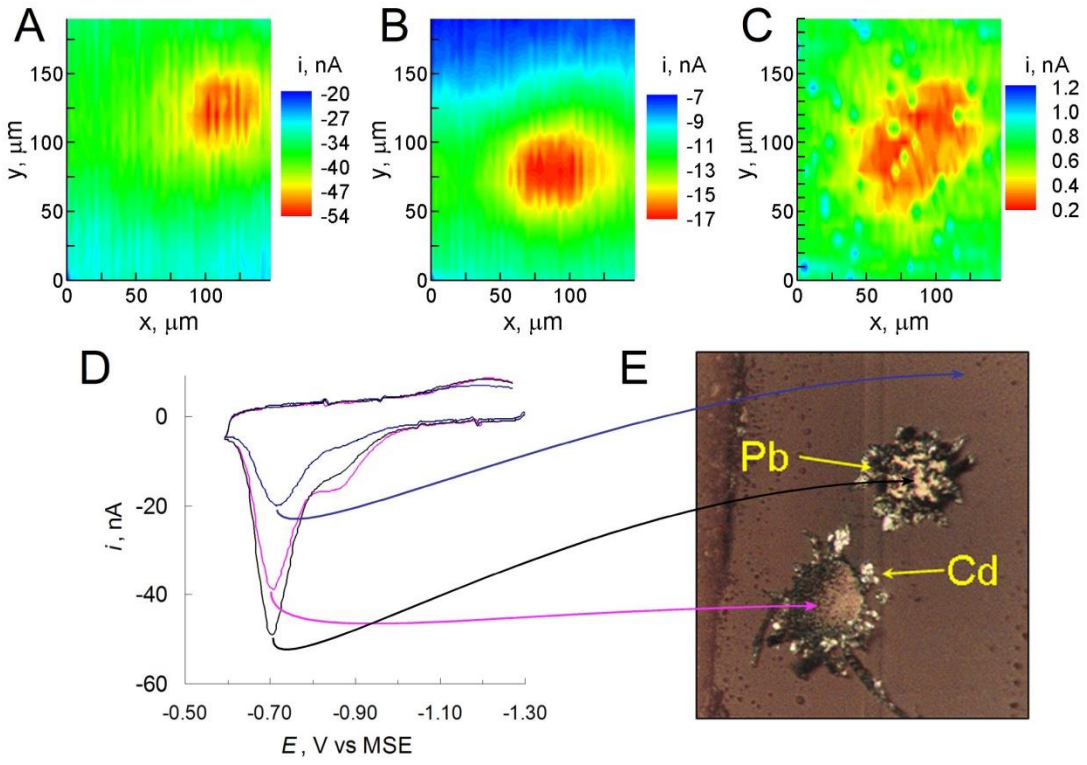

Figure 6. (A), (B), and (C) ASV-SECM images at a dual 25 µm diam Pb and Cd electrode for Pb^{2+}, Cd^{2+}, and O_2, respectively. (D) Extracted ASVs from the image data at different positions of the scan as indicated by arrows on (E), an optical micrograph of the surface. Tip-substrate distance of 6 µm (see text for additional details)

Interestingly, no metal dissolution from the substrate is expected at the imaging potential of –1.30 V vs. MSE used to acquire the data in Figure 6. The Nernst equation (1) for a metal in equilibrium with its ion predicts that the ion concentration will be much

$$E = E^{o\prime} + \frac{RT}{nF}\ln[\mathrm{M}^{n+}] \qquad (1)$$

smaller than micromolar at the potential used here. Thus, the micromolar ion concentrations observed are anomalous. One possible explanation is that dissolved O_2 is reduced on the Pb, Cd, or on exposed Pt metal surface producing H_2O_2, which chemically oxidizes both Pb and Cd. This explanation is consistent with the lower concentration of

O_2 over both Pb and Cd as observed in Figure 6C. While no attempt was made to detect peroxide, the method could in principle be adapted to detect and quantify H_2O_2 and even other intermediaries relevant to electrocatalysis.

We feel, however, that a more likely explanation for the high metal ion concentration is due to an induced dissolution process.[29, 30] As the tip scans above the metal substrate electrodes it removes the solution-phase metal ions near the electrode. This shifts the equilibrium potential of the metal to a more negative value, forcing additional metal dissolution.

An example showing the role induced dissolution plays in producing image contrast is shown in Figure 7. The figure shows ASV-SECM images of a segment of 100 μm diam Pt substrate biased at –600 mV vs. Ag/AgCl in a solution of 1 μM Pb^{2+} and Cd^{2+}. The image was acquired by collecting a voltammogram every 2 μm along the *x* axis while raster scanning at 3.5 μm/s, giving a preconcentration time of 575 ms. Steps along the *y* axis were 10 μm.

The two images are separate false-color plots of the current data from the anodic part of the ASV. Figure 7A, with E_t = –698 mV, corresponds to a map of O_2 (E_t = –698 mV) while 7B is a map of Pb^{2+}, with E_t = –397 mV (vs. Ag/AgCl). The O_2 image shows that the image region is of only the left hemicircle of the substrate. At E_{sub} = –600 mV, the substrate should reduce O_2 and the metal ions within and extending somewhat beyond the substrate perimeter. Under these conditions, the tip current due to O_2 is smaller (i.e. lowered cathodic current) over the substrate, as expected due to a depletion effect at the substrate.[5]

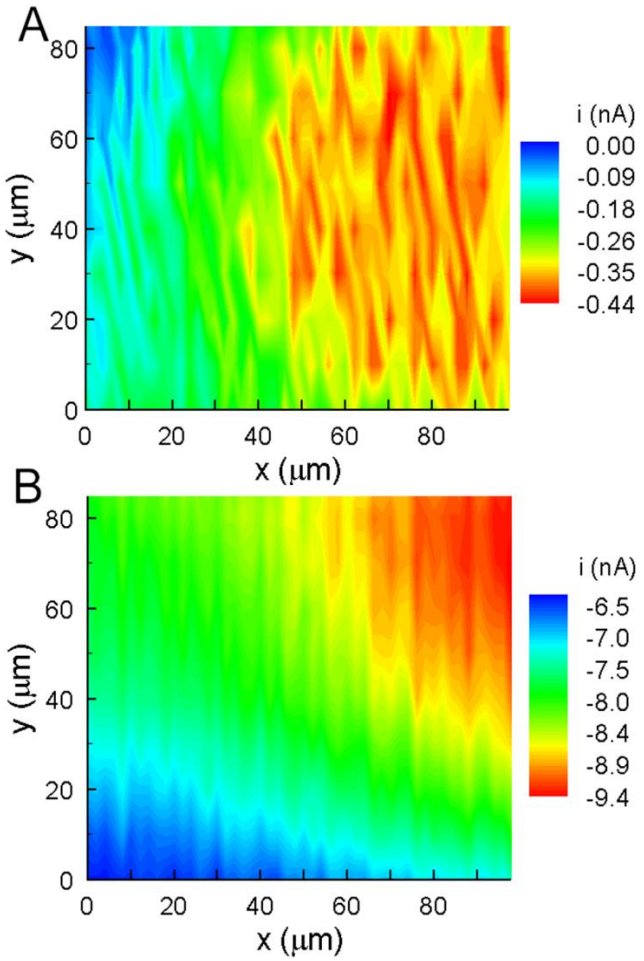

Figure 7. ASV-SECM image at a 100 μm diam Pt disk in a 1 μM Pb^{2+}, Cd^{2+} using a 10 μm diam Hg-Pt film tip with a tip-substrate separation of ca. 10 μm. Images show the currents from the anodic part of the ASVs: (A) E_t = –698 mV, O_2 reduction and (B) E_t = –396 mV, Pb. All potentials vs. Ag/AgCl, t_p = 575 ms, v = 100 V/s

In Figure 7B the region over the substrate shows higher anodic tip currents for the Pb ASV peak even though the concentration of Pb^{2+} ions must be lowered near the substrate due to reduction to the metal at the substrate potential. However, the substrate is also becoming covered with Pb (and Cd) during the course of the imaging experiment. The scanning tip is also reducing metal ions and consequently depleting the solution above the substrate electrode. As a result, Pb^{2+} and Cd^{2+} ions are produced by the

substrate to restore equilibrium conditions. Integration of the difference between the Pb stripping peak current from a voltammogram above the Pb-coated Pt electrode (*x*, *y* position = 100, 90 µm) and a voltammogram at the beginning of the scan (0, 0) gives a net peak charge of 1.44 pC, which can be ascribed to the amount of Pb^{2+} induced to dissolve from the Pb-coated substrate (see Figure S-4). This amount of charge corresponds to about 2.5 pA of current flowing over the preconcentration time of 0.575 s.

This level of current is easily supplied by a tip-sized region of the substrate if we consider the rate at which equilibrium can be established following perturbation by the tip. The cathodic and anodic part of the $Pb^{2+/0}$ equilibrium will take place at a finite rate as estimated from the Butler-Volmer equation (2), written in terms of the current density, *j*, and ignoring mass transport limitations:

$$j = j_c - j_a = j_0\left\{\exp[-\alpha nf(E - E_{eq})] - \exp[(1-\alpha)nf(E - E_{eq})]\right\} \qquad (2)$$

Where j_a and j_c is the anodic and cathodic current densities, j_o is the exchange current density, α is the apparent transfer coefficient and $f = F/RT$ = 38.9 V^{-1} (at 25 °C). Kinetic parameters for the reduction of Pb^{2+} were found in the literature (α = 0.8).[31] We found $E^{0'}$ by potentiometric measurements of *E* vs. Pb^{2+} concentration for a Pb wire vs. MSE (Figure S-5).[6] Fitting to equation 2 gave an $E^{0'}$ of –347 vs. Ag/AgCl. The resulting estimates of j_a, j_c, and j_o were computed for the experimental overpotentials found here and are presented in Table S-1.

This shows the high sensitivity of the ASV-SECM method. These results strongly suggest that the ASV-SECM technique could be used to measure the dissolution reaction even under potentials where a net electrodeposition occurs (i.e., at negative overpotentials). In contrast, it would be difficult to detect a net dissolution current of

2.5 pA in a standard SECM experiment due to the background processes. The images here are noisy and reflect an earlier experimental setup. Some of the noise was removed in later experiments by grounding the metal table and stage of the SECM. Although work is still in progress to improve the signal to noise ratio, the fact that the substrate is visible in Figure 7 suggests that will be possible to improve the limit of detection below micromolar levels.

Underpotential Deposition (UPD) Imaging An image of a 25 μm diam electrode at E_{sub} = –300 mV vs. Ag/AgCl with a 10 μm diam, Hg-covered Pt disk provides an interesting experimental result (Figure 8). The test solution is 20 μM $Cd(NO_3)_2$/ 20 μM $Pb(NO_3)_2$/ 0.5 M KNO_3. At E_{sub} = –300 mV, bulk Pb or Cd is not thermodynamically stable on the electrode surface. In Figure 8, the image is a region 120 × 120 μm, the *x*-step is 3 μm, the scan rate is 5 μm/s with a preconcentration time, t_p = 600 ms. The tip-substrate separation, *d*, is estimated to be ca. 5 μm from an approach curve using O_2 reduction at E_{sub} = 0 mV. The substrate appears as a region of low cathodic current in the O_2 reduction image (A, E_t = –698 mV), but as region of a higher anodic currents at the Cd^{2+} (B, E_t = –480 mV) and Pb^{2+} (C, E_t = –303 mV) stripping peak potentials. The imaged region surrounding the substrate provides a baseline comparison of the tip currents. Since the substrate electrode is well positive of the potential required to reduce Pb^{2+} or Cd^{2+} to bulk metal, induced metal dissolution as described above does not apply. What, therefore, accounts for the apparent metal ion increase over the substrate surface?

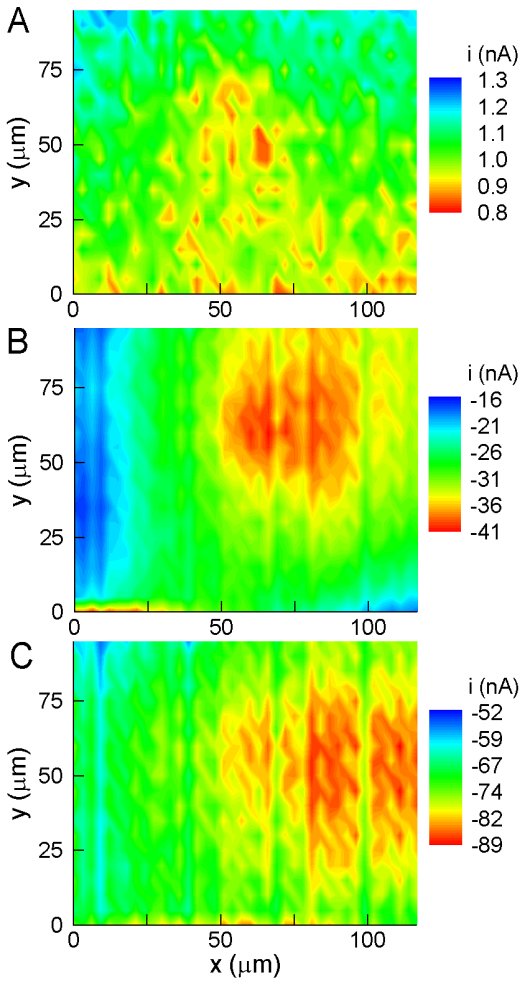

Figure 8. ASV-SECM images of a 25 μm diam Pt disk substrate (E_{sub} = –300 mV) in 20 μM Pb^{2+} and Cd^{2+} acquired with a 10 μm diam Hg-Pt film tip at a tip-substrate separation of about 5 μm. Concentration maps of (A) O_2, E_t= –698 mV; (B) Cd^{2+} E_t = –480 mV; and (C) Pb^{2+} E_t = –304 mV, were obtained from the same surface scan. All potentials vs. Ag/AgCl, t_p = 600 ms, v = 100 V/s.

At potentials positive of the thermodynamic equilibrium potential for the $M^{n+/0}$ system, UPD deposition can usually proceed until a monolayer (ML) of the metal has deposited on the substrate electrode. For Pb and Cd, the difference between the equilibrium potential and the monolayer equilibrium potential, ${}_{ML}\Delta E$, has been reported for polycrystalline Pt as ~0.87 V for Pb^{2+}/Pt and ~0.96 V for Cd^{2+}/Pt.[32] For Cd^{2+}/Pb,

$_{ML}\Delta E = 0$, which discards the possibility of UPD of Cd over Pb, and of a full Pb monolayer. Based on the $_{ML}\Delta E$ values found in the literature, the equilibrium of the monolayer potential, $_{ML}E_{eq}$ was calculated for each of the metals and was found to be +374 mV vs. Ag/AgCl for Pb^{2+}/Pt and +187 mV vs. Ag/AgCl for Cd^{2+}/Pt. The value of the substrate potential in Figure 8 is more negative than both of these potential values for ML deposition, so it is possible to have UPD of Pb and Cd at the Pt substrate.

Subtracting voltammograms taken at a region away from the Pt electrode from voltammograms atop the Pt electrode and deconvoluting the Pb and Cd peaks, a total stripping charge of 20 pC was determined to be due to the effect of the substrate. Table 3 shows the results for two positions, (60, 60) μm and (90, 60) μm, over the Pt substrate, along with the equivalent steady state current that must flow during the preconcentration time (600 ms) to supply this charge.

It is clear that the charge available from the dissolution of one monolayer, Q_{ML}, is more than enough to provide the ca. 20 pC needed to account for the increment in the peak current for both Pb and Cd over the Pt substrate as observed in Figure 8. This confirms that the tip is removing sub-monolayer amounts, ca. 1% of the ML coverage of Pb and Cd on Pt.

We have also considered the effect of surface diffusion at the substrate as a component of the stripping charge seen in the experiment of Figure 8. For the case of an SECM tip electrolyzing a chemical species and depleting a surface region of radius r_0, a surface diffusional flux will arise to replenish this region. Thus, the steady-state tip current ascribed to surface diffusion, $i_{D,sur}$, will be given by equation 3:[33]

$$i_{D,sur} = \frac{2\pi nFD_{sur}(\Gamma^* - \Gamma_0)}{\ln(r_1 / r_0)} \quad (3)$$

where D_{sur} is the surface diffusion coefficient (Table 3) and Γ^* and Γ_0 are the surface coverage at $r = r_1$ and r_0, respectively.

Evaluation of equation 3 requires knowledge of the regions with boundary conditions of Γ^* and Γ_0. The region with a depleted coverage Γ_0 is the region under the scanning tip. This region is given by the *resolution function* (4),[34] so r_0 will be:

$$r_o = a + 1.5d \quad (4)$$

For the conditions in Figure 8, r_0 = 13.25 μm. This radius completely covers the radius of the substrate electrode. The value of r_1 is taken to be that of the glass surrounding the electrode, which is $r_1 = 10a$ = 50 μm. Further, we set $\Gamma_0 = 0$ and Γ^* to complete monolayer coverage, 1.6 and 2.15 nmol/cm^2; based on the density of Pb and Cd, respectively. These assumptions will overestimate the surface diffusion flux under the conditions here. The $i_{D,sur}$ calculated is shown in Table 3.

Table 3. Comparison of the stripping peak charge (Q_p), expected induced dissolution current (i_{ss}), UPD monolayer charge (Q_{ML}), and maximum possible surface diffusion contribution ($i_{D,surf}$) under conditions of Figure 8

	ASV at (60, 60) μm		**ASV at (90, 60) μm**		Q_{ML}	$i_{D,sur}$
	Q_p (pC)	**i_{ss} (pA)**	**Q_p (pC)**	**i_{ss} (pA)**	**(pC)**	**(pA)**
Pb	17.3	28.8	25.4	42.4	1520	0.365
Cd	20.8	34.7	23.8	39.7	2040	530

The amount of Pb^{2+} supplied by surface diffusion is not enough to account for the observed Pb signal. However, the Cd surface diffusion current is in the range that can account for the increment of this metal. Since $i_{D,sur}$ values have been greatly overestimated, we think that the charge due to UPD Cd dissolution is still most likely

responsible for the Cd current. We note that the effect of surface diffusion on the dissolution process may become more apparent with larger substrates, where our assumptions about surface diffusion will become more realistic.

In Figures 7 and 8 the metal ion images show higher concentration because the tip forces the dissolution of the metals when the mass transport to the tip from the bulk of the solution is hindered. To further illustrate the effect of the mass transport of the metal ions to the tip and substrate, two ASV imaging scans of 120×100 μm acquired with the same *x*-step (3 μm) and preconcentration time (600 ms) as in Figure 8, but with a much larger tip-substrate separation, *d*, ca. 15 μm and at two different substrate potentials (–300 and –700 mV vs. Ag/AgCl), Figure 9. The images from the scan for E_{sub} = –300 mV are (A), O_2 E_t = –698 mV; (B) Cd^{2+} E_t = –446 mV and (C) Pb^{2+} E_t = –263 mV. The metal ion images (Figures 9B and 9C) do not show the increased contrast and higher currents seen when *d* is ca. 5 μm over the substrate electrode (cf. Figures 8B and 8C); here the stripping currents seem to increase mainly as a consequence of the sample tilt, follow the same trend as the increase in O_2 reduction current seen in Figure 9A (no O_2 reduction) with only a slight increase in the Pb oxidation current in the area close to the substrate electrode. This is expected, because the Nernst equation (1) predicts a shift of the reduction potential to more negative values at lower concentration of the metal ion (M^{n+}):

When the potential of the substrate is set to –700 mV, the currents for O_2 reduction (D, E_t = –698 mV), Cd^{2+} (E, E_t = –422 mV), and Pb^{2+} (F, E_t = –261 mV) are smaller than those in (A), (B), and (C), which is consistent with the fact that the substrate is depleting the solution at this very negative potential. The oxygen reduction current (Figure 9D) shows the region above the substrate electrode as a much smaller current

range; a similar trend is seen in the oxidation current of Cd (Figure 9E), with smaller stripping currents over the region of the substrate electrode. For the Pb stripping image, the currents are much smaller and there is little image contrast.

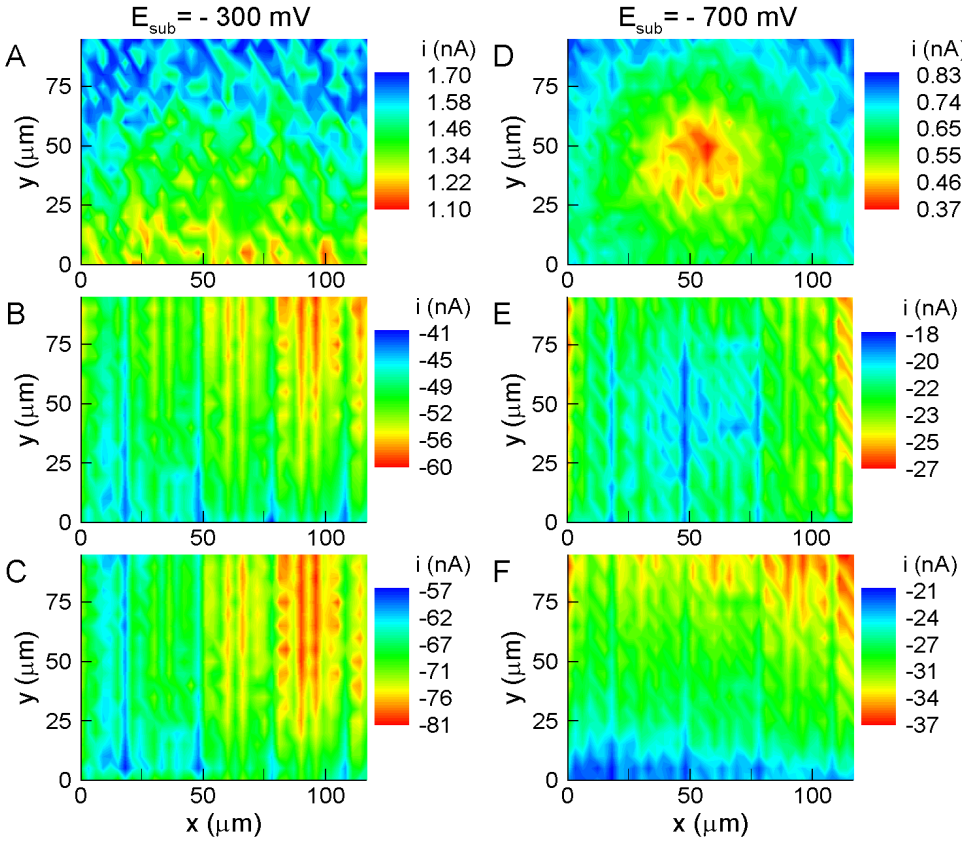

Figure 9. ASV-SECM images of a 25 μm diam Pt disk at E_{sub} = –300 mV and –700 mV in 20 μM Pb^{2+} and Cd^{2+} with a 10 μm diam Hg-Pt film tip at a tip-substrate separation of about 15 μm. Concentration maps for E_{sub} = –300 mV are (A) O_2, E_t = –698 mV; (B) Cd^{2+} E_t = –446 mV; and (C) Pb^{2+} E_t = –263 mV, were obtained from the same surface scan. A different imaging experiment for E_{sub} = –700 mV is shown in (D) O_2, E_t = –698 mV; (E) Cd^{2+} E_t = –422 mV; and (F) Pb^{2+} E_t = –261 mV. All potentials vs. Ag/AgCl, t_p = 600 ms, v = 100 V/s.

In summary, Figures 7, 8, and 9 show that the different imaging conditions (E_{sub}, d, C*) over the same region can change the appearance of the substrate because different phenomena dominate the experiment. It is particularly interesting that an apparent increase in metal ion concentration is observed under conditions when the mass transport

to the tip-sample gap is sufficiently hindered (e.g. Figure 7 and 8) and that induced dissolution can be observed at both bulk metal and UPD layers.

Conclusion

The use of a voltammetric mode of imaging in SECM has greatly expanded its capability. In this work, the addition of fast-scan ASV to SECM provides sensitive and selective imaging of multiple chemical species at interfaces immersed in solution. This is demonstrated by showing that a single ASV-SECM image can produce unique concentration maps indicating Cd^{2+} and Pb^{2+}, generated *in situ* from a corroding sample, while simultaneously detecting the depletion of O_2 at this sample. Fast scan anodic stripping currents are shown to be linear for 1-100 μM of Pb^{2+} and Cd^{2+} solutions using a preconcentration time of 300 ms and stripping scan rates of 100 V/s. SECM images are presented indicating that metal ion concentrations as low as 1 μM are observed. Increasing the signal-to-noise ratio seems to be possible by increasing the stripping scan rate, which has the dual effect of isolating the signal from the power line noise and increasing the peak current.[13] Further optimizing the experiment by employing more efficient analog and digital filtering should permit FS-ASV SECM to image multiple chemical species at nanomolar levels.

We expect that the ASV-SECM method will find applications for examination of environmental samples, sensitive mapping of localized metallic corrosion precursor events, and trace metal ion interactions with biological and polymeric material. In addition, the demonstrated ability to locally observe UPD processes and possibly metal ion surface diffusion suggests new applications for the study of potential-driven adsorption phenomena at metallic and other surfaces. Future quantitative studies under

these imaging conditions will require simulations that include dissolution kinetics from the Hg amalgam and surface diffusion rates or UPD coverage of the metals.

Voltammetric SECM methods should provide greater flexibility than those previously used in SECM since it should now be possible to adapt existing anodic, cathodic, and other adsorptive stripping methods to allow sensitive imaging of a number of previously inaccessible chemical species with the SECM method.[35]

Acknowledgement

This work was supported by the National Science Foundation (DBI-9987028), the State of Mississippi, and Mississippi NSF-EPSCoR program (EPS-9874669).

Supplementary Material

Available: Additional stripping voltammograms, Pb equilibrium data, calculated Pb deposition rates, tip characterization, and simulation details (14 pages) are available as Supporting Information. Current ordering information is found on any masthead page.

References

(1) Bard, A. J.; Fan, F.-R.; Mirkin, M. V. In *Electroanalytical Chemistry*; Bard, A. J., Ed.; Marcel Dekker: New York, 1994; Vol. 18, pp 250.
(2) Bard, A. J.; Mirkin, M. V., Eds. *Scanning Electrochemical Microscopy*; Marcel Dekker: New York, 2001.
(3) Schrock, D. S.; Wipf, D. O.; Baur, J. E. *Anal. Chem.* **2007**, *79*, 4931-4941.
(4) Schrock, D. S.; Baur, J. E. *Anal. Chem.* **2007**, *79*, 7051-7053.
(5) Diaz-Ballote, L. F.; Alpuche-Aviles, M.; Wipf, D. O. *J. Electroanal. Chem.* **2007**, *604*, 17-25.
(6) Zhou, F.; Aronson, J. T.; Ruegnitz, M. W. *Analytical Chemistry* **1997**, *69*, 728-733.
(7) Wu, H. P. *Anal. Chem.* **1994**, *66*, 3151-3157.
(8) Wu, H. P. *Anal. Chem.* **1996**, *68*, 1639-1645.
(9) Sawamoto, H.; Gamoh, K.; Nishiuchi, R. *Bunseki Kagaku* **1991**, *40*, 499-501.
(10) Munoz, E.; Palmero, S.; Garcia-Garcia, M. A. *Electroanalysis* **2000**, *12*, 774-777.
(11) Golimowski, J.; Krasnodebska-Ostrega, B. *Fresenius' J. Anal. Chem.* **1998**, *361*, 65-68.
(12) Brainina, K. Z.; Bond, A. M. *Anal. Chem.* **1995**, *67*, 2586-2591.
(13) Munteanu, G. G.; Munteanu, S. G. *J. Anal. Chem.* **2006**, *61*, 266-272.
(14) Muntyanu, G. G. *J. Anal. Chem.* **2004**, *191*, 91-100.
(15) Baranski, A. S. *Anal. Chem.* **1987**, *59*, 662-666.
(16) Penczek, M.; Stojek, Z. *J Electroanal. Chem.* **1985**, *191*, 91-100.
(17) Daniele, S.; Bragato, C.; Ciani, I.; Baldo, M. A. *Electroanalysis* **2003**, *15*, 621-628.
(18) Daniele, S.; Ciani, I.; Bragato, C.; Baldo, M. A. *J. Phys. IV* **2003**, *107*, 353-356.
(19) Janotta, M.; Rudolph, D.; Kueng, A.; Kranz, C.; Voraberger, H.-S.; Waldhauser, W.; Mizaikoff, B. *Langmuir* **2004**, *20*, 8634-8640.
(20) Rudolph, D.; Neuhuber, S.; Kranz, C.; Taillefert, M.; Mizaikoff, B. *Analyst* **2004**, *129*, 443-448.
(21) Ruhlig, D.; Schuhmann, W. *Electroanalysis* **2007**, *19*, 191-199.
(22) Wightman, R. M.; Wipf, D. O. In *Electroanalytical Chemistry*; Bard, A. J., Ed.; Marcel Dekker: New York, 1989; Vol. 15, pp 267-353.
(23) Scharifker, B.; Hills, G. *J. Electroanal. Chem.* **1981**, *130*, 81-97.
(24) Baldo, M. A.; Daniele, S.; Mazzocchin, G. A. *Electrochim. Acta* **1996**, *41*, 811-818.
(25) Kolpakova, N. A.; Borisova, N. V.; Nevostruev, V. A. *J. Anal. Chem.* **2001**, *56*, 744-747.
(26) Guminski, C.; Galus, Z. In *Metals in Mercury*; Hirayama, C., Galus, Z., Guminski, C., Eds.; Pergamon Press: Oxford, 1986; Vol. 25, pp 330-334.
(27) Bath, B. D.; Michael, D. J.; Trafton, B. J.; Joseph, J. D.; Runnels, P. L.; Wightman, R. M. *Anal. Chem.* **2000**, *72*, 5994-6002.
(28) Baur, J. E.; Kristensen, E. W.; May, L. J.; Wiedemann, D. J.; Wightman, R. M. *Anal. Chem.* **1988**, *60*, 1268-1272.
(29) Macpherson, J. V.; Unwin, P. R. *J. Phys. Chem.* **1995**, *99*, 3338-3351.
(30) Macpherson, J. V.; Unwin, P. R. *J. Phys. Chem.* **1996**, *100*, 19475-19483.

(31) Hampson, N. A.; Larkin, D. *Trans. Faraday Soc.* **1969**, *65*, 1660-1667.
(32) Kolb, D. M. In *Advances in Electrochemistry and Electrochemical Engineering*; Gerischer, H., Ed.; John Wiley and Sons: New York, 1978; Vol. 11, pp 125-172.
(33) Lie, L. H.; Mirkin, M. V.; Hakkarainen, S.; Houlton, A.; Horrocks, B. R. *Journal of Electroanalytical Chemistry* **2007**, *603*, 67-80.
(34) Bard, A. J.; Mirkin, M. V.; Unwin, P. R.; Wipf, D. O. *J. Phys. Chem.* **1992**, *96*, 1861-1868.
(35) Wang, J. *Stripping Analysis: Principles, Instrumentation, and Applications*; VCH Publishers: Deerfield, FL, 1985.
(36) Bard, A. J.; Faulkner, L. R. *Electrochemical Methods: Fundamentals and Applications*, 2nd ed.; John Wiley and Sons: New York, NY, 2000.
(37) Heyrovsky, J.; Kuta, J. In *Principles of Polarography*; Academic Press: New York, 1966, pp 106-107.
(38) Martins, M. E.; Salvarezza, R. C.; Arvia, A. J. *Electrochim. Acta* **1995**, *41*, 2441-2449.